DOE/ER/13033--T1

Final Report

MIGRATION OF FISSION PRODUCTS IN UO_2

University of California at Berkeley

DOE Award No. DE-FG02-90er13033

RECEIVED
NOV 17 1995
OSTI

Principal Investigators:

S. G. Prussin and D. R. Olander

ABSTRACT

The results of an experimental and calculational effort to examine the fundamental mechanisms of fission product migration in and release from polycrystalline uranium dioxide are reported. The experiments were designed to provide diffusion parameters for the representative fission products tellurium, iodine, xenon, molybdenum and ruthenium under both reducing and oxidizing conditions. The calculational effort applied a new model of fission product release from reactor fuel that incorporates grain growth as well as grain boundary and lattice diffusion.

DISCLAIMER

This report was prepared as an account of work sponsored by an agency of the United States Government. Neither the United States Government nor any agency thereof, nor any of their employees, makes any warranty, express or implied, or assumes any legal liability or responsibility for the accuracy, completeness, or usefulness of any information, apparatus, product, or process disclosed, or represents that its use would not infringe privately owned rights. Reference herein to any specific commercial product, process, or service by trade name, trademark, manufacturer, or otherwise does not necessarily constitute or imply its endorsement, recommendation, or favoring by the United States Government or any agency thereof. The views and opinions of authors expressed herein do not necessarily state or reflect those of the United States Government or any agency thereof.

MASTER

DISTRIBUTION OF THIS DOCUMENT IS UNLIMITED DLC

I INTRODUCTION

This work addresses experimental measurements of migration parameters of characteristic fission products in stoichiometric and oxidized UO_2 and presents a calculational model to assess the effect of fuel microstructure on fission product release in a more fundamental manner than heretofore available for fuel behavior analysis.

The concentrations and spatial distributions of fission products bred into reactor fuel and their behavior under a wide range of physical and chemical conditions are key parameters in in-core fuel performance, reactor safety under normal operating conditions and for assessing radiological hazards from different types of reactor accidents. The migration in and release of the volatile fission products from UO_2 during normal operation define the inventories of radionuclides which contribute to pellet-cladding interaction(PCI) and which are available for quick release in the event of cladding failure. Under accident conditions, transport of fission products defines the source term for radiological hazard estimations.

Notwithstanding the importance of transport properties and the substantial effort expended in the past on the study of migration and release characteristics of the rare gases krypton and xenon, knowledge of the transport of most other fission products is rudimentary, both with respect to a fundamental understanding migration on an atomic scale or with respect to gross release properties of the fuel. Such topics were reviewed by the NSF/NRC Workshop on Chemical Processes and Products in Severe Reactor Accidents(1). This study pointed to the need for improved definition of the release characteristics of nuclides which present the greatest radiological burden under the full range of conditions expected in postulated accidents(2). The majority of the migration parameters in codes such as VICTORIA(3) designed to model the course of various accident scenarios and to assess their radiological consequences have not been measured experimentally.

What measurements do exist have been obtained by analysis of release data using the Booth equivalent sphere model(4). By its very nature, this model contains no reference to the real microstructure of the fuel and thus provides only a correlation applicable to the particular material studied and under the given experimental conditions. Thus the parameters derived with the Booth model are applicable only to a small range of conditions likely to be found in real accident scenarios. The series of severe fuel damage tests at the PBF facility at INEL have shown that the Booth model predictions underestimate fission gas release during the heatup phase of an accident where "diffusive" release occurs(5). Fuel morphology is a dominant factor in this phase.

The experimental program conducted here is concerned with measurement of the transport of representative fission products in well-characterized polycrystalline UO_2 in a manner which permits estimation of migration parameters both within grains and along grain boundaries. Elements were chosen which span all of the major classes of fission products with respect to significant release fraction, chemistry(both within the fuel and after releases) and radiological consequences. By control of the gaseous atmosphere, the diffusion properties were measured under conditions which are associated with a range of postulated accident types.

Successful extension of the burnup of LWR fuels to 50 - 60 GWD/t(average) depends critically on the fission gas release characteristics of the fuel. Burnup may be limited by gas pressure buildup in the fuel element. Japanese research at NFD is developing modified UO_2 for this purpose. The fuel will have a much larger grain size than current fuels to reduce fission product release and will contain additives such as Nb to promote fuel plasticity(6).

Another concern with extended-burnup operation of LWR fuel is operability of the rods with breached cladding. Water entering failed rods oxidizes a portion of the fuel, which in turn enhances fission product release. The effect of hyperstoichiometry on fission product release has been studied in this work with steam-oxidized pellets with O/U ratios up to 2.2(but still with the fluorite crystal structure). In addition, the effect of simultaneous oxidation and fission product release has been studied.

In previous experiments conducted in this laboratory, the technique of post-irradiation annealing has been used to investigate the release characteristics of Te, I, Xe, Cs, Ba and the refractories Ru, Mo, and Tc. In all cases the fuel was stoichiometric, with an average grain size of 6 - 10 μm, and the data was interpreted in terms of the Booth model(4). While effective diffusivities and activation energies for most species were generally consistent with previous measurements in the literature, the activation energies for Mo and Tc migration were factors of 2 - 4 times larger(7). This results points to considerably greater complexity in the migration/release process of these elements than for the true volatiles.

With the development of a realistic model of impurity migration which explicitly accounts for both grain-boundary and volume diffusion in polycrystalline materials(8), we developed a chemical microsectioning procedure which permits measurement of concentration profiles of fission products after high-temperature annealing(9). This procedure yields distributions with a resolution of some tens of microns, which is sufficient to extract in-grain and grain-boundary diffusion coefficients for most of the elements noted above.

II EXPERIMENTAL STUDIES

We have utilized the post-irradiation annealing method and the chemical microsectioning method to study release of the volatile fission products from trace-irradiated UO_2 and UO_{2-x} specimens in controlled atmospheres. Three sets of conditions were used:

(a) Stoichiometric UO_2, constant morphology and composition: These experiments were intended to provide data on in-grain and grain-boundary migration parameters. Measurements were performed on well-characterized, as-fabricated fuel specimens under conditions of limited grain growth. Trace-levels of fission products were studied. Some of the fuel was subjected to high-temperature annealing prior to irradiation in order to measure diffusion parameters of material of identical composition but different grain sizes.

(b) Stoichioimetric UO_2 under conditions of grain growth: Under conditions encountered during the in-core lifetime of fuel, significant grain growth can occur near the centerline of the fuel. This set of experiments was designed to estimate differences in the diffusion properties in the

same fuel material as in (a) but with annealing at sufficiently high temperatures to produce significant grain growth during the release of the fission products.

(c) Release from hyperstoichiometric fuel: Fractional releases were measured from initially hyperstoichiometric material which had been annealed in a steam environment to produce UO_{2+x}, with $2.05<x<2.20$. These experiments were conducted in an apparatus equipped with a microbalance to follow any changes in the oxidation state of the specimen during the anneal that released fission products

The equipment used in the experiments consists of vacuum furnaces, sample handling equipment, microbalances, and ceramographic equipment. All radioactivity measurements were performed with high-resolution gamma-ray spectrometry to provide multi-element analyses on each annealed specimen.

Results

(a) Analysis of Fission Product Profiles

The chemical microsectioning technique of Ref. 9 was used to measure the concentration profiles of representative fission products in UO_2 of 20 μm average grain size following post-irradiation annealing. Profiles were obtained for isotopes of Mo, Ru, I, Te, and Ba, and the distributions were fitted to the model given in Ref. 8, for which equilibrium segregation of the solute to the grain boundaries is assumed. The experiments and model fits also provided fractional release data from which standard Booth effective diffusion coefficients could be calculated. The data from these measurements were also analyzed to provide the best estimates of the volume diffusion coefficient, D_V, and the product of tne grain-boundary segregation coefficient and the grain-boundary diffusivity, HD_{gb}.

Modeling efforts were undertaken to better understand the transport properties obtained in the experiments. Rather than assuming equilibrium segregation(which clearly is inappropriate for insoluble species such as Xe), the data were analyzed assuming irreversible trapping at the grain boundaries. A comparison of the transport parameters derived with the two assumptions provided insight into the model dependency of the parameters(particularly D_V) and the magnitudes of the grain-boundary segregation coefficients for the soluble fission products such as Mo.

(b) Effect of Fuel O/U and Grain Growth on Fission Product Release

Fission product release from oxidized fuel is important both in normal operation with a cladding breach as well as during the fuel degradation stage of a severe reactor accident. During normal operation, some cladding tubes are breached due to processes such as PCI or debris fretting. When this occurs, steam fills the fuel-cladding gap. Although pure steam oxidizes UO_2 only very slowly at typical fuel periphery temperatures, the presence of reactive species caused by radiolysis of the steam in the gap by recoiling fission fragments(e.g., H_2O_2) accelerates fuel

oxidation. The oxidized fuel more easily releases fission products and contributes to the radioactivity of the coolant.

In a severe accident, the cladding balloons at ~1000°C and fails, providing a large opening for steam access to the fuel. At ~ 1300°C, fuel oxidation by steam becomes rapid, and the oxidized fuel releases fission products more readily than stoichiometric fuel.

The present work examined the release of the fission products Te, I, Ru, Mo and Xe from fuel with O/U ratios of 2.00, 2,08, and 2.20. The specimens were trace-irradiated in a reactor to provide the initial quantity of trapped fission products. The gamma-ray spectrum of the irradiated specimens was measured before and after annealing in a high-temperature furnace. From these measurements, the fractional release of the five fission products was determined from the decrease in the height of their characteristic gamma-ray peaks. The fractional release was converted to the effective diffusion coefficient by the Booth equation(4):

$$f_{rel} = \frac{6}{\sqrt{\pi}}\sqrt{\frac{Dt}{a^2}}$$

Alternatively, the true lattice diffusion coefficient, D_V and the grain-boundary diffusion coefficient D_{gb}, were determined from experiments using the same material but of different specimen thicknesses. In this case, the model of Ref. 8 was used to interpret the data.

Figure 1 shows a summary plot of the results based on the Booth model approach. Here, the effective diffusion coefficients of the five fission products tracked in the experiment are shown for two fuel stoichiometries at two temperatures. In stoichiometric fuel, tellurium is the most readily released, probably because it occupies anion lattice sites in the fuel and thus diffuses at a rate similar to that of O^{2-}, which is very fast compared to cation diffusion. Note that even the refractory elements Mo and Ru exhibit measurable releases. Contrary to expectations, Xe is the least mobile of all of the fission products studied.

At 1200°C, the effect of oxidizing the fuel from UO_2 to $UO_{2.20}$ causes increases in the effective diffusion coefficient by as much as six orders of magnitude(for Mo and Ru). The reason for this substantial effect is that the oxidized fuel creates volatile species such as MoO_3 and RuO_4, whereas in stoichiometric UO_2, these species exist either as metal or a lower oxide, either of which is much less volatile than the highly-oxidized forms. At 1700°C, the effect of oxidation is much less striking, and the effective diffusion coefficients are within an order of magnitude of each other at a fixed O/U ratio.

Figure 2 shows the temperature dependence of the true lattice diffusion coefficient of Te(determined by analyzing the data according to the model of Ref. 8). As the O/U ratio increases, the activation energy for diffusion and the pre-exponential factor both decrease. The former effect predominates, and the effect of oxidation is to increase the lattice diffusivity by several orders of magnitude.

Fig. 1

Effective Diffusion Coefficients of Volatile Fission Products in Fuel

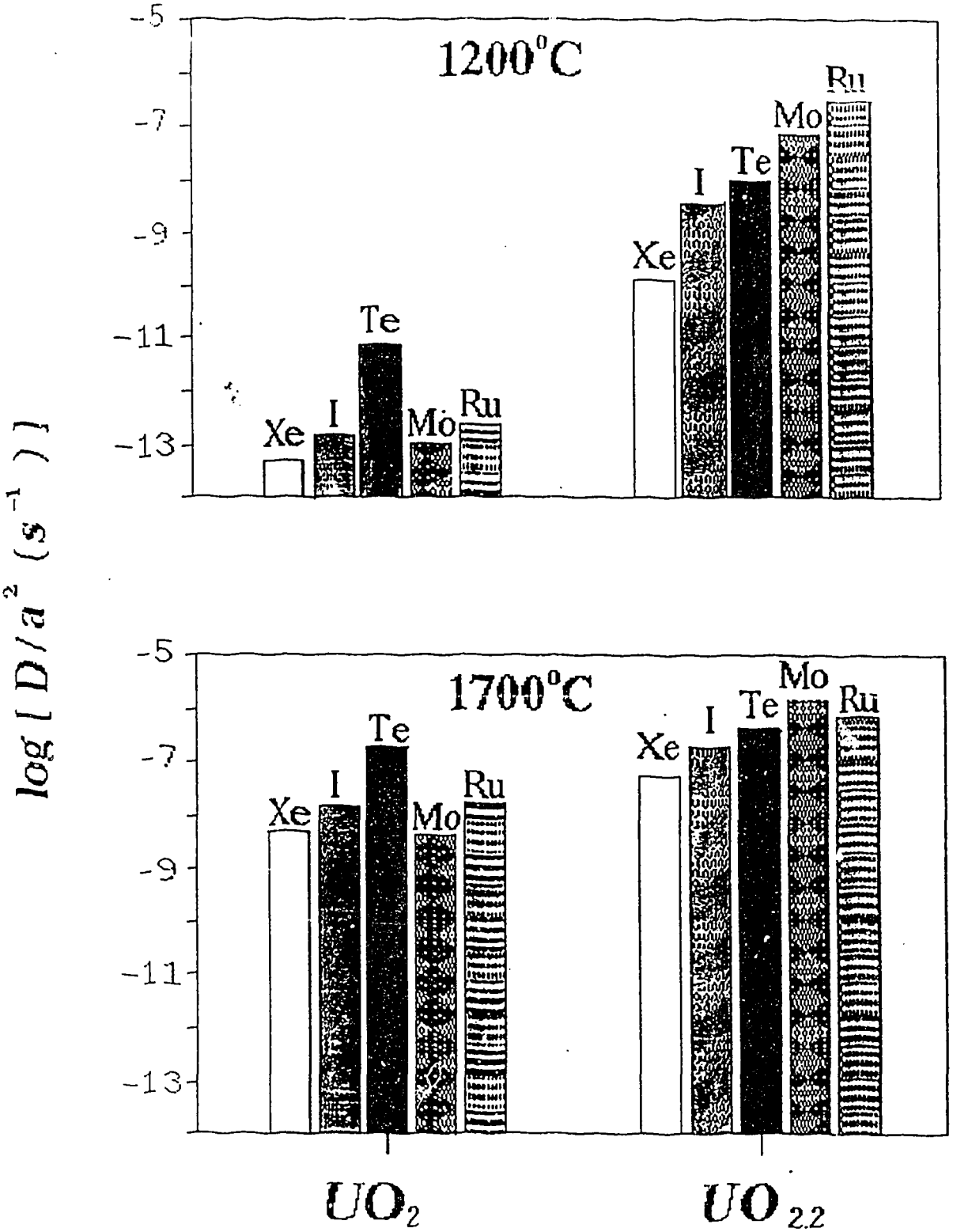

Fig. 2

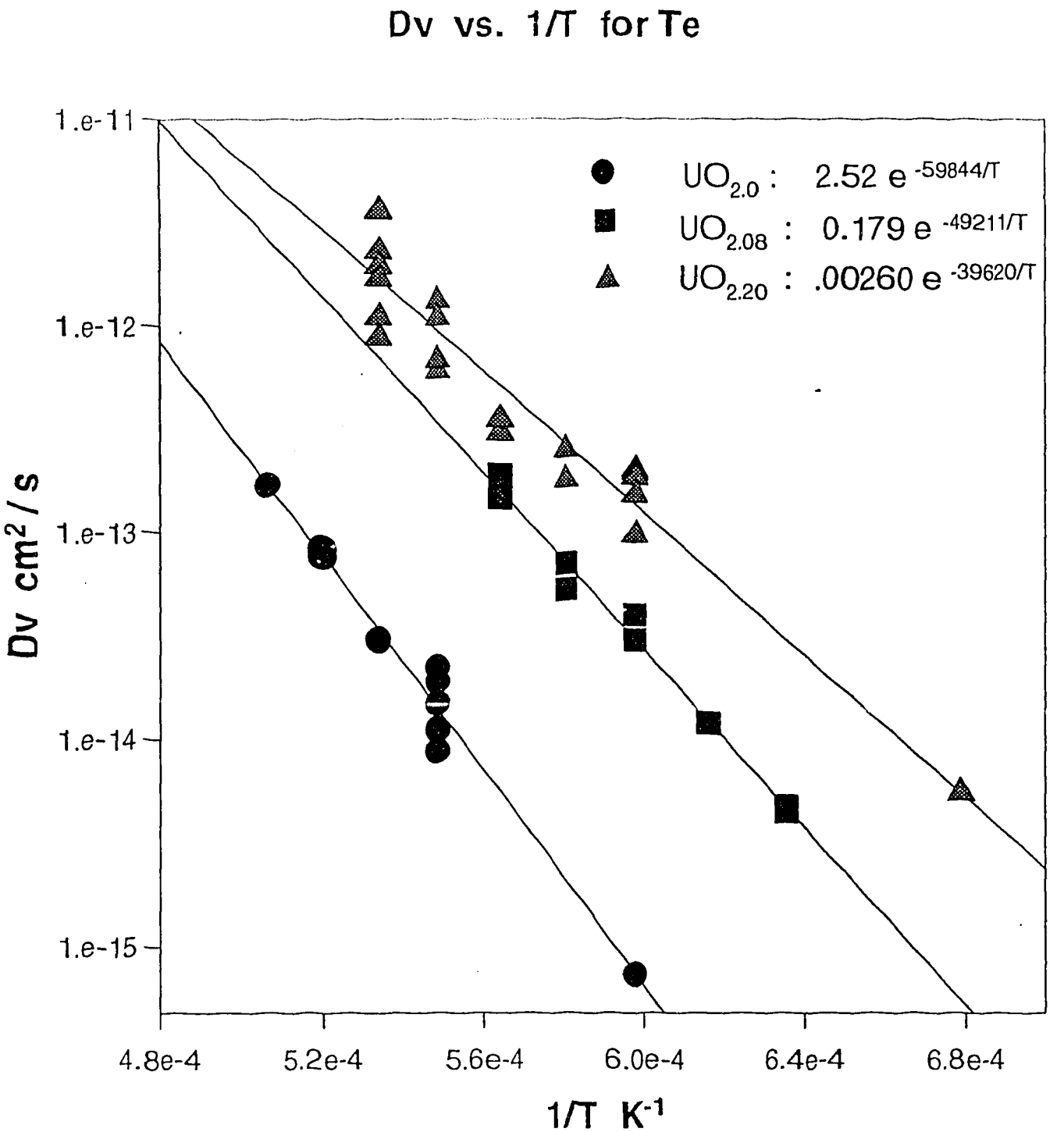
Dv vs. 1/T for Te
1.e-11
1.e-12
1.e-13
1.e-14
1.e-15
Dv cm² / s
UO2.0 : 2.52 e -59844/T
UO2.08 : 0.179 e -49211/T
UO2.20 : .00260 e -39620/T
4.8e-4
5.2e-4
5.6e-4
6.0e-4
6.4e-4
6.8e-4
1/T K-1

III THEORETICAL MODELING

Existing models of fission gas release either neglect the co-occurring phenomenon of grain growth or treat it in an unrealistic manner(i.e., as a "sweeping" process). In reality, this process must be considered as a combination of grain-boundary and lattice diffusion with simultaneous movement of the grain boundaries. The approach contained two steps.

(a) The Slab-grain model

In the first approach, the classical(Fisher/Whipple) model of coupled grain boundary and lattice diffusion was extended to account for the movement of the grain boundary during penetration of a surface-deposited solute. This model represents the grain boundaries as infinite thin slabs normal to the surface. Such an approximation is valid for metals, with large grain size and small penetration distances during diffusion, but is not directly applicable to bodies such as sintered UO_2. However, the geometrical simplicity of the Fisher-Whipple grain boundary representation makes it ideal for development of mathematical models and analytical testing of the advanced model incorporation boundary motion.

Application of the moving-boundary theory to the classical Fisher-Whipple picture also provides a valuable side product. For over 30 years, experimental studies of grain boundary diffusion have used the classical model for data interpretation. In many of these cases the temperature range of the diffusion experiments extended into the temperature range at which grain growth takes place. Thus, the data analysis should have considered grain boundary movement. We have applied the moving-boundary model to re-analyze literature data for tracer diffusion in pure lead with the aim of deducing the correct grain boundary diffusion coefficient by properly accounting for boundary movement during penetration. A detailed description of the model is given in Attachment 1.

(b) The Spherical -grain model

The second part of the modeling effort dealt with fission gas release from a realistic fuel microstructure, in which the diffusion distance was many grain diameters and in which the grains were simulated as spheres. Fission gas release from a microstructure with a distribution of grain sizes undergoing grain growth was analyzed. Hillert's theory was used to describe the evolution of the grain morphology, during which some grains enlarge while others shrink and may even disappear. Limiting cases of booth release(when only diffusion occurs) and Malen release(when grain-boundary movement is dominant) were derived for a body with a distribution of grain sizes. The moving boundary diffusion equation that couples the diffusion and sweeping mechanisms was derived and solved numerically; the grain-size distribution was divided into 25 groups for which diffusion equations are solved for the average intragranular gas concentration. The results were compared to existing single-grain-size models, which, in all cases, overpredict the fractional release. Details of this analysis are presented in Attachment 2.

IV REFERENCES

1. National Research Council Report on the Workshop on Chemical Processes and Products in Severe Reactor Accidents, South Seas Plantation, Captiva Island, FL, Dec 1987

2. Ibid, report of Panel C, "Heterogeneous Kinetics of Release of Radioactive Species from Fuel"

3. W. J. Camp, "Release of Fission Products from Reactor Fuels During Severe Accidents: The VICTORIA code:, Sandia Nat'l Laboratory Report SAND87-2929C(1987)

4. A. H. Booth, Atomic Energy of Canada Report AECL-496(1957)

5. D. J. Osetek et al, "Behavior of Fission Products from Severely Damaged Fuel during the PBF Severe Fuel Damage Tests", Proc., 5th Internat. Mtg. on Thermal Reactor Safety, Karlsruhe, (1984)

6. D. R. Olander, Paper presented at the Japan Technology Evaluation Center(JTEC) Nuclear Power Workshop, (1990)

7. S. G. Prussin, D. R. Olander, W. K. Lau and L. Hansson, J. Nucl. Mater., **154**, 25 (1988)

8. D. R. Olander, Adv. in Ceramics, **17**, 271 (1986)

9. F. Osaisai, S. G. Prussin, and D. R. Olander, J. Nucl. Mater., **173**, 149 (1990)

V Publications resulting from the project

PhD Theses:

U. E.-Saied, " The Role of Grain Boundary Diffusion and Movement in the Process of Fission Gas Release" (1993)

M. Mansouri, " Release of Volatile Fission Products from Oxidized Urania" (1995)

Journal Articles:

D. R. Olander and U. M. El-Saied, "The Effect of Grain Boundary Motion on the Kinetics of Solute Penetration into a Polycrystalline Medium", Acta Metall. Mater., **40**, 1329(1992)

U. El.-Saied and D. R. Olander, " Fission Gas Release during Grain Growth in a Microstructure with a Distribution of Grain Sizes", J. Nucl. Mater., **207**, 313 (1993)

M. Mansouri and D. R. Olander, "Fission Product Release Kinetics in $UO_{2\pm x}$", J. Nucl. Mater., submitted

ATTACHMENT 1

THE EFFECT OF GRAIN BOUNDARY MOVEMENT AND SURFACE DIFFUSION ON THE SOLUTE PENETRATION OF POLYCRYSTALLINE SOLIDS.

I INTRODUCTION

The mathematical analysis of the grain boundary diffusion process began with Fisher [1] who studied the effect of coupling diffusion in the lattice with grain boundary diffusion on the solute penetration into a polycrystalline solid. Whipple [2] and Suzuoka [3] extended this work by obtaining exact solutions using the Laplace-Fourier transform method. The difference between the two analyses is in the choice of the boundary condition at the surface. Whipple assumed a constant concentration of solute at the surface at all times. This is physically realized only if the layer of solute-containing material that is deposited on the substrate is immiscible with the polycrystalline material. If this is so, the layer is an a phase rich in solute A in equilibrium with substrate phase b rich in solvent B as specified by the phase diagram of the A-B binary. The interface between the layer and the substrate falls in the two-phase region of the A-B phase diagram. The surface concentration used in Whipple's analysis is the solubility of A in the b phase and remains constant as long as the a phase is present on the surface.

However, when the layer and the substrate form a solid solution, or when the two phases are the same element and the solute is radioactive isotope of the element, the Fisher-Whipple boundary condition does not apply. Suzuoka assumes a more realistic model by adopting a zero-solute flux condition at the surface coupled with an initial distribution representing a thin, finite source at the surface. This boundary condition is also used in analysis of solute penetration of single crystals. Solute diffusion along the surface will act as a source of the solute to the mouth of the grain boundary and Suzuoka's condition of zero solute flux perpendicular to the surface needs modification.

Fisher's, Whipple's and Suzuoka's analyses, in common with all subsequent studies of this problem [4-5], assume the grain boundary to be stationary. On the other hand, at elevated temperature the grain boundaries move, making some grains grow and the others shrink. Glaeser and Evans [6] first recognized the potential importance of grain boundary movement in assisting solute penetration

into a polycrystalline solid. They showed that with this mechanism operating, volume diffusion is not needed to produce solute penetration into the lattice. Introducing grain boundary movement in the analysis does not mean that the grain growth problem was properly coupled in the model. In considering grain boundary movement, the size and shape of the grains are assumed to remain constant while the boundaries are displaced. In grain growth, on the other hand, boundary movement is accompanied by enlargement of grains of larger-than-average size and shrinkage of smaller ones.

The Fisher-Whipple-Suzuoka analysis and that of Glaeser and Evans represent limiting cases of the general phenomenon of solute penetration of a solid by the combined effects of grain boundary diffusion, lattice diffusion, grain boundary movement and surface diffusion. In an earlier work [7], the authors presented a model which combines the first three processes. In this work we review theoretical efforts to combine the above four processes in a general model.

The classical experiment for determining grain boundary diffusion coefficients involves coating the surface of a polycrystalline specimen with a radioactive isotope of the element (solute) and annealing for a fixed time at a constant temperature. Thin slices of the specimen are then removed sequentially and analyzed for their solute contents. The depth profile of the solute exhibits a rapid initial decrease which is determined by direct lattice diffusion from the surface followed by a flatter deep-penetration portion that depends on two properties of the polycrystalline specimen. The ordinate level of this curve (or the scale) depends principally on the grain size and grain morphology of the specimen. The slope of the deep-penetration part of the distribution is governed mainly by the combined grain thickness - grain boundary diffusion coefficient parameter δD_{gb}, the boundary velocity V and the surface transport parameter $\delta_S D_S$.

The experimental solute depth profile represents the average concentration of solute in the lattice at time t as a function of depth y. The average concentration according to the theoretical models, assuming a cubical grain of side length d, is described by:

$$\overline{C} = \frac{4}{d}\int_0^{\infty} C(x,y,t)dx = KF(y,t) \qquad (1)$$

where x is the lateral distance from the grain boundary and y is the distance along the grain boundary taking the surface as the origin. The x-integral is carried from x=0 (at the grain boundary) to $x=\infty$. The latter limit requires that the average lateral penetration depth be small compared to the grain size. K is called the *scale factor* and F is the *shape function*. For all the models, the scale factor is expressed as:

$$K = \frac{8}{\sqrt{\pi}}\frac{\sqrt{Dt}}{d} \qquad (2)$$

where D is the bulk diffusion coefficient. The magnitude of the scale factor K in the above equation is not of interest because it is not dependent on the mobility of the solute in the grain boundary. The lateral integral F contains the desired information, so all theories concentrate on predicting this function. When plotted as $\ln\overline{C}$ vs. $y^{6/5}$, both the Whipple and Suzuoka theories predict linear behavior. The grain boundary mobility parameter D_{gb} is obtained from the slope of this line beyond the range of direct lattice diffusion from the surface. The shape functions here are independent of the choice of the surface condition [8]. However, the scale factors deduced from the experimental data are different for the Whipple and Suzuoka models. Suzuoka [3] showed that the scale factor obtained by fitting data on Co penetration into Fe implies, by equation (2), a grain size that agrees with the observed grain size. Treatment of the same data by Whipple's model gives the same value of D_{gb} but a significantly larger apparent grain size. This indicates that the finite-source boundary condition is a more accurate representation of the surface behavior than is the constant-concentration boundary condition.

II THE MOVING-BOUNDARY MODEL

In the moving boundary model of grain boundary-assisted penetration of a solute into a polycrystalline solids, the grain boundary is assumed to move parallel to the surface with velocity V. As the grain boundary moves, it collects the solute ahead of it and redeposits solute behind it. The concentration of the solute ahead of the grain boundary is different from that behind it and two bulk diffusion equations are needed. In this analysis we will use dimensionless parameters to describe the spatial and time variables. X,Y and τ are related to the physical parameters by:

$$X = \frac{x}{E} \quad , \quad Y = \frac{y}{E} \quad , \quad \tau = \frac{Dt}{E^2} \tag{3}$$

where:

$$E = \frac{\delta D_{gb}}{2D} \tag{4}$$

is a characteristic length. δ is the thickness of the grain boundary and D_{gb} is the solute diffusion coefficient in this region. X and X′ are the dimensionless lateral distances ahead and behind the grain boundary, respectively. Using the dimensionless parameters of equation 3, the bulk diffusion equations are [7]:

$$\frac{\partial C}{\partial \tau} = \frac{\partial^2 C}{\partial X^2} - A\frac{\partial C}{\partial X} \tag{5}$$

$$\frac{\partial C'}{\partial \tau} = \frac{\partial^2 C'}{\partial X'^2} + A\frac{\partial C'}{\partial X'} \tag{6}$$

C and C′ are the concentrations ahead and behind the grain boundary, respectively. The Y-direction diffusion term can be neglected as long as the depth-time combination $Y/\tau^{1/4}$ is larger than ~3 and $\tau <\sim 10^{-3}$ [8]. The last term in both equations is the convective term due to grain boundary movement. A is the boundary velocity parameter:

$$A = \frac{VE}{D} \tag{7}$$

The grain boundary diffusion equation is:

$$G\frac{\partial C}{\partial \tau} = \frac{\partial^2 C}{\partial Y^2} + \frac{1}{2}\left(\frac{\partial C}{\partial X} + \frac{\partial C'}{\partial X'}\right) \quad , \quad at\ X = X' = 0 \tag{8}$$

where C_{gb} is the concentration in the grain boundary. And:

$$G = \frac{D}{D_{gb}} \tag{9}$$

G represents the ratio of the diffusivity in the bulk to the diffusivity in the grain boundary and it is in the range of 10^{-4} to 10^{-6}. In the quasi-stationary approximation, G can be set equal to zero.

The initial condition is:

$$C = C' = 0 \quad , \quad at \quad \tau=0 \tag{10}$$

and the boundary conditions are:

$$C = C' \quad , \quad at \quad X=0 \tag{11}$$

$$C = C' = 1 \quad , \quad at \quad Y=0 \tag{12}$$

$$C = C' = 0 \quad , \quad at \quad X=Y=\infty \tag{13}$$

The part-analytic, part-numerical solution method of the coupled lattice and moving grain boundary diffusion equations is given in Ref. 7. As A approaches 0, this solution agrees well with the Whipple shape function:

$$F_w = \frac{Y}{\sqrt{\tau}} \int_0^1 exp\left(-\frac{Y^2 s^2}{4\tau}\right)\left[\frac{e^{p^2}}{\sqrt{\pi}} - p\, erfc(p)\right] ds \tag{14}$$

where

$$p = \frac{1}{2}\left(\frac{1}{s^2} - 1\right)\sqrt{\tau} \tag{15}$$

As A -> ∞, the Glaeser-Evans solution [6] is recovered:

$$F_{GE} = \frac{A\sqrt{\pi\tau}}{2} exp\left(-\sqrt{\frac{A}{2}}Y\right) \tag{16}$$

Figure 1 shows the solutions for a range of the boundary-movement parameter A. The approximate solution provides an accurate interpolation method between the two analytic limiting cases. The regions in which each solution is valid are shown below:

Range of $A\tau^{1/2}$	**Model**
<~1	Whipple
~1 to ~4	Present
>~4	Glaeser-Evans

The serial-sectioning technique applied to polycrystalline specimens with an initial solute deposit on the surface yields the profile of the lateral-average solute concentration as a function of depth at a fixed time. The grain boundary mobility parameter δD_{gb} is determined from such data by the following method:

1. D, t, and V are specified. The lattice diffusivity D is determined by independent methods on single-crystal material. The boundary velocity is estimated from grain-growth data.

2. The parameter E of equation(4) is guessed. This determines A of equation (7) and τ of equation (3) and allows the data to be expressed as $\overline{C}_{exp}(Y)$

3. The mean-square deviation of $\overline{C}_{exp}(Y)$ from KF(Y,τ) for all data points is minimized by adjusting the scale factor K.

4. Steps 2 and 3 are repeated using different values of E. The value that produces the lowest mean-square deviation is the value that best fits the data.

Applying this method to the experimental data of Gupta and Kim [9] on the tracer-lead deposit/natural-lead substrate system using the grain growth data reported by Drolet and Galibois [10] showed that the value of δD_{gb} implicit in the tracer penetration data is approximately five times larger than that obtained by interpreting the data using the Whipple method for stationary grain boundaries.

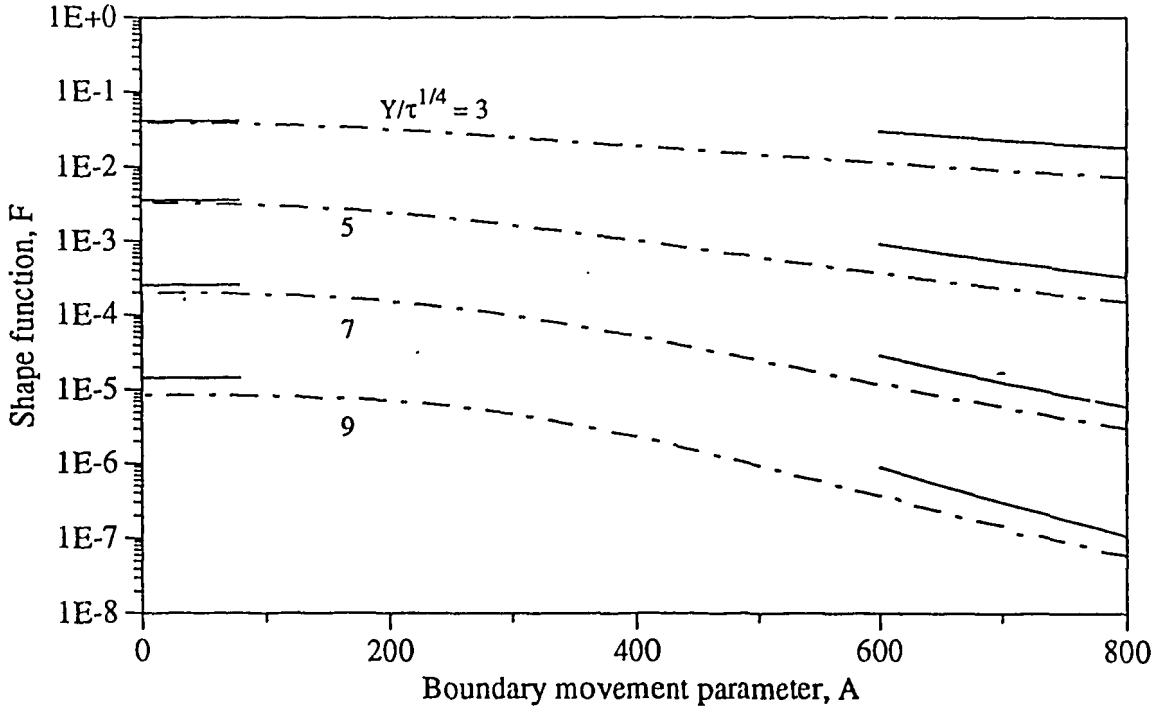

Figure 1. Shape function for solute penetration of a polycrystalline solid with a moving boundaries. Dot-dash curves: approximate solution of ref. [7]; horizontal solid lines: Whipple solution for A=0; and solid curves: Glaeser-Evans solution for A->∞. The dimensionless time τ is 10^{-4}; for various time-depth variables $Y/\tau^{1/4}$.

III Effect of Surface Diffusion

In analyzing solute penetration experiments on single-crystal substrates using the finite-source boundary condition requires the surface boundary condition:

$$\left(\frac{\partial C}{\partial Y}\right)_{Y=0} = 0 \qquad at \quad all\ X\ and\ \tau \tag{17}$$

There is no question concerning the validity of equation (17) when the substrate is a single crystal containing no localized high-diffusivity pathways intersecting the surface. However, for tracer penetration into a polycrystal, the situation at the surface is more complicated. In his analysis, Suzuoka [3] states that its use requires assuming that "the rate of flow along the surface be of the same order of magnitude as that in the medium", which is equivalent to assuming that the surface diffusion coefficient

is zero. In Suzuoka's model, the only source of solute to the grain boundary is via lattice diffusion from the surface a distance several units of $\sqrt{Dt}$ removed from the grain boundary. The lattice diffusion process supplies solute to the grain boundary up to approximately the same depth. Thereafter, the grain boundary acts as a source of solute feeding the lattice and produces the characteristic deep-penetration tail observed in the $\overline{C}_{exp}(Y)$ distribution measured in the serial-sectioning method.

Solute can also be fed to the mouth of the grain boundary by diffusion along the surface. The equation governing this process is:

$$\delta_S \frac{\partial C_S}{\partial t} = \delta_S D_S \frac{\partial^2 C_S}{\partial x^2} + D\left(\frac{\partial C_S}{\partial y}\right)_{y=0} \tag{18}$$

where C_S is the concentration of solute on the surface and δ_S is the thickness of the region in which surface diffusion takes place. It is roughly equal to the lattice spacing in the crystal, and thus is of the same order of magnitude as δ. Equation 18 is identical in form to the grain boundary diffusion equation with x and y interchanged, δ replaced by δ_S, and D_{gb} replaced by D_S. Neglecting the time derivative in equation (18) because δ_S is very small and expressing the spatial coordinates in dimensionless terms yields:

$$0 = S\frac{\partial^2 C}{\partial X^2} + \frac{\partial C}{\partial Y} \quad \cdot \quad at \qquad Y=0 \tag{19}$$

where

$$S = 2\left(\frac{\delta_S D_S}{\delta D_{gb}}\right) \tag{20}$$

If S is small, equation (19) reduces to equation (17), which is the condition employed by Suzuoka [3]. At the other extreme, if S>>1, equation (20) requires that $\partial^2 C/\partial X^2$ on the surface. Since $\partial C/\partial X$ as X -> ∞, this limit implies that C is everywhere constant on the surface.

If D_S and D_{gb} are known, S can be estimated and the appropriate limit determined. For example, the coefficients of self diffusion and grain boundary diffusion for copper are known [11,12]. Using these data and assuming $\delta_S = \delta$, S is about 20 at 1000 K and about 30 at 800 K. This suggests that surface diffusion is a significantly more efficient source of solute for the grain boundary than is lattice diffusion from the surface layer. Thus, the opposite limiting surface boundary condition from that employed by Suzuoka is more appropriate for this system. In order to analyze the grain-boundary transport problem in this limit, the surface concentration must be known as a function of time.

Examination of experimental solute penetration profiles obtained by the serial sectioning technique shows that essentially all solute is removed from the initial surface deposit by direct lattice diffusion to the underlying substrate; the quantity of solute contained in the deep-penetration portion of the distribution, which is due to diffusion along the grain boundary, is small by comparison. Therefore the appropriate surface boundary condition for the analysis when S>>1 is exactly the same as that used for single crystals, namely:

$$C(X,0,\tau)) = \frac{W}{\sqrt{\pi\tau}} \tag{21}$$

where W is proportional to the strength of the surface source. At the mouth of the grain boundary(X=Y=0), Suzuoka's solution gives a concentration which is about a factor of 5-10 smaller

than that given by equation (21). The result of rapid surface diffusion is to increase the driving force for diffusion into the grain boundary by a comparable factor.

The problem addressed by Suzuoka with replacement of the surface boundary condition of equation(17) by that of equation(21) can be solved by the Fourier-Laplace method.

V CONCLUSIONS

The results presented here demonstrate the importance of including grain boundary movement and surface diffusion in analyzing the process of solute penetration in the bulk. Small grain boundary motion enhances solute transport into the solid but large velocities hinder deep penetration. Analysis of experimental measurements using the appropriate shape function is needed to account for grain boundary movement as well as surface diffusion during the experiment. As both of these processes are thermally activated, the temperature range of the penetration experiments may fall in the region where grain growth or surface diffusion is important. The solution when both boundary movement and surface diffusion occur during solute penetration has not yet been solved.

REFERENCES

[1] Fisher , J., J. of App. Phy., 1951,22, 74.
[2] Whipple , R., Phil. Mag., 1954, 45, 1225.
[3] Suzuoka , T., Trans. of the Japanese Institute of Metals, 1961, 2, 25.
[4] Oishi , Y. and Ichimura, H. ,J. Chem. Phys., 1979, 71, 5134.
[5] Olander , D., Advances in Ceramics, 1986, 17, 271.
[6] Glaeser , A. and Evans , J., Acta Metall. Mater., 1986, 34, 1545.
[7] Olander, D. and El-Saied, U. , Acta Metall. Mater.,1992, 40, 1336.
[8] Le Claire, A., Brit. J. Appl. Phys., 1963, 14, 351.
[9] Gupta , D. and Kim, K., J. of App. Phy., 1980, 51, 2066.
[10] Drolet , J. and Galibois , A., Acta Metall. Mater., 1968, 16, 1387.
[11] Kaur, I. , Gust W. and Kozma, L., "Handbook of Grain and Interface Boundary Diffusion Data.", Ziegler press., Stuttgart, 1989, vol. 1, p 380.
[12] Bonzel, H., Surf. Sci., 1970, 21, 45.

ATTACHMENT 2

FISSION GAS RELEASE BY DIFFUSION IN THE PRESENCE OF GRAIN GROWTH

I Introduction

In early work, fission gas release was treated as a diffusional problem in fixed-size spheres of a specified equivalent radius[1]. Many other mechanisms affecting release were subsequently added to the models, including that due to grain boundary sweeping which occurs at temperatures at which grain growth is significant. Since fission gas is totally insoluble in the fuel matrix, a moving grain boundary collects all gas in the lattice ahead of it but does not redeposit any in the newly-formed crystal behind it. In effect, the moving grain boundary acts as a fission gas filter.

The current treatment of this phenomenon is summarized here. Basically, the gas accumulation terms due to ordinary diffusion from within the grain and from grain boundary sweeping are derived separately and then added. The grain boundary sweeping term, due to Hargreaves and Collins[2], is derived first.

Consider a unit area of grain boundary moving into solid with fission gas concentration $\overline{C}$. Since diffusion is not considered, the fission gas concentration is assumed to be uniform throughout the grain, at least before the grains start to grow. In time dt, the grain boundary moves a distance $\dot{R}$dt, where $\dot{R}$ is the grain boundary velocity. The term $\dot{R}$dt is also the volume per unit grain boundary area swept in dt. The number of fission gas atoms in this volume, $\overline{C}\dot{R}\,dt$, accumulate in the grain boundary. If φ is the areal concentration of fission gas in the grain boundary, $d\phi = \overline{C}\dot{R}\,dt$, or:

$$\left(\frac{d\phi}{dt}\right)_{gbs} = \overline{C}\dot{R} \qquad (1)$$

where the subscript *gbs* denotes grain boundary sweeping.

The grain boundary velocity in Eq(1) is determined from the observed rate of change of the

average grain radius with time:

$$\dot{R} = \frac{d\overline{R}}{dt} \tag{2}$$

where $\overline{R}$ is determined from the grain growth law. For the common case of parabolic grain growth:

$$\overline{R}^2 - \overline{R}_0^2 = kt \tag{3}$$

where k is the parabolic grain growth constant. The grain size is determined microscopically by counting the number of intersections with grain boundaries in a unit length of line on a photomicrograph, P_L[3]:

$$2\overline{R} = \overline{L}_3 = \frac{1}{P_L} \tag{4}$$

Figure 1 shows the basis of this method.

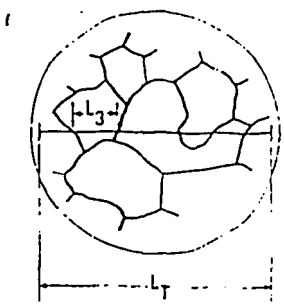

Fig. 1 Method for determining the average grain size of a polycrystal[3]

Diffusional release of fission gas to the grain boundary is described by the diffusion equation. For the case of post-irradiation annealing with an initially uniform gas concentration C_o in the solid,

$$\frac{\partial C}{\partial t} = \frac{D}{r^2}\frac{\partial}{\partial r}\left(r^2\frac{\partial C}{\partial r}\right) \tag{5}$$

where the initial condition is:

$$C = 1 \qquad \text{at} \qquad t = 0 \tag{6}$$

and the boundary condition is:

$$C = 0 \qquad \text{at} \qquad r = R \tag{7}$$

This equation is solved *neglecting motion of the boundary* and solved for the concentration distribution C(r,t). The diffusional flux of fission gas atoms to the boundary is:

$$\left(\frac{d\phi}{dt}\right)_{diff} = -D\left(\frac{\partial C}{\partial r}\right)_R \tag{8}$$

where D is the diffusion coefficient of fission gas in the lattice.

The total rate of accumulation of fission gas in the grain boundaries is assumed to be the sum of the two contributions[4]:

$$\frac{d\phi}{dt} = \left(\frac{d\phi}{dt}\right)_{diff} + \left(\frac{d\phi}{dt}\right)_{gbs} \tag{9}$$

The time rate of change of the number of fission gas atoms in a grain is given by:

$$\frac{d}{dt}\left(\frac{4}{3}\pi R^3 \overline{C}\right) = -4\pi R^2\left[\left(\frac{d\phi}{dt}\right)_{diff} + \frac{1}{2}\left(\frac{d\phi}{dt}\right)_{gbs}\right] \tag{10}$$

where:

$$\overline{C} = \frac{3}{R^3}\int_0^R r^2 C\, dr \tag{11}$$

The factor of one half in front of the last term on the right hand side reflects the fact that only the growing grain appears to lose gas by accumulating gas-free solid as the grain boundary moves; the adjacent shrinking grain does not lose fission gas but its size diminishes. Neglecting the time dependence of R, Eq(10) is:

$$\frac{d\overline{C}}{dt} = \frac{3D}{R}\left(\frac{\partial C}{\partial r}\right)_R - \frac{3\overline{C}\dot{R}}{2R} \tag{12}$$

The fractional release of the fission gas to the grain boundary in time t is:

$$f_{r,gb} = 1 - \overline{C} \tag{13}$$

Additional impediments to gas release to the environment, such as diffusion in the grain boundary or formation of grain-boundary bubbles, are not considered here.

The above analysis suffers from two major defects. First, grain growth is a far more complex process than simply the expansion of the average grain size. The radius R is usually taken to be the average grain size determined from microscopic examinations of cut sections of the polycrystalline fuel. In reality, some grains grow and some shrink. In the period of observation, some disappear entirely. Figure 2 shows this process schematically. The shrinking grains(some marked with a minus sign) have less than 5 sides in a 2-D representation and the growing grains have six or more sides(marked with plus signs in Fig. 2). Grains become triangular just before disappearing(in 3-D, they are tetrehedra just before disappearing). None of this detail is contained in Eq(1).

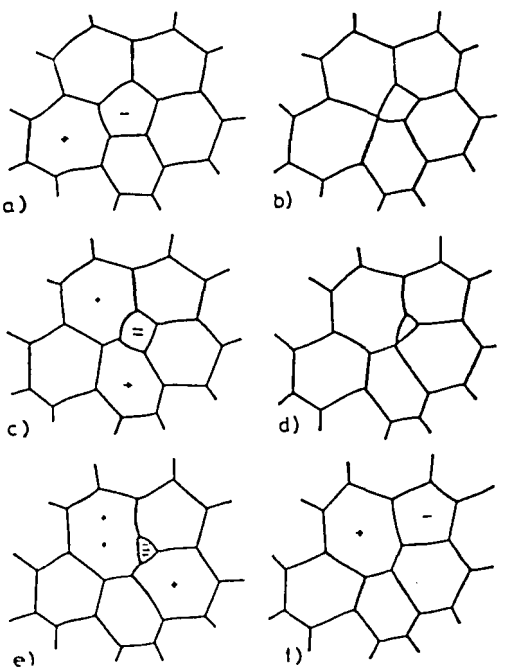

Fig. 2 Evolution of the grain structure from time zero(a) through later times

Second, in solving Eq(5) for the diffusive contribution to release, the radius R in Eq(7) is assumed to be time-independent. This is incorrect and calculations based on this assumption can be in significant error.

II GRAIN GROWTH KINETICS

Grain morpholog, is described by the size distribution function F(R), where F(R)dR is the fraction of grains with radii between R and R+dR. The evolution of this distribution function is the central problem of grain growth theory. A sketch of this process is shown in Fig. 3. In general, grains with radii less than a critical value R_c tend to shrink initially and those with larger radii tend to grow. Simultaneously, the number of grains per unit volume and their internal surface area decrease with time.

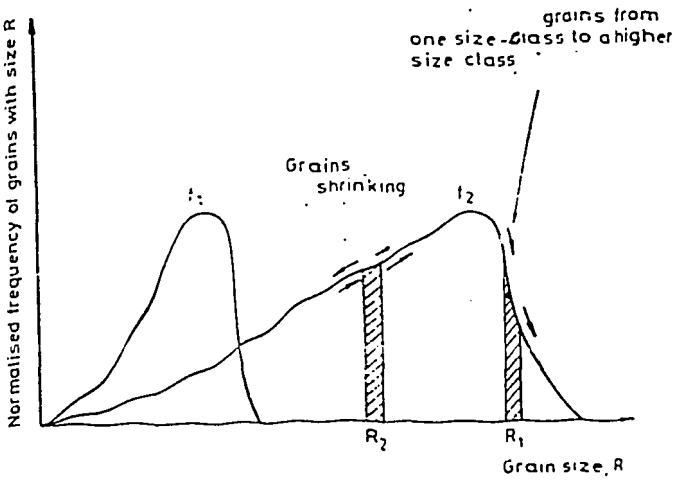

Fig. 3 Change in the grain size distribution function with time

Various methods of dealing with the problem theoretically are reviewed by Atkinson[5]. The approach adopted here is called the mean field approach. This method deals with the change in size of an isolated grain embedded in an environment which represents the average effect of the entire array of grains. Feltham[6] and Hillert[7] have presented analyses based upon this model and Hunderi and Rhun[8] have further refined them. The basic physical property is the growth rate of individual grains. Hillert proposed that this quantity is described by:

$$\frac{dR^2}{dt} = M\left(\frac{R}{R_c} - 1\right) \tag{14}$$

where M is a growth rate constant that is proportional to the product of the mobility of the grain boundary and the surface energy of the boundary. According to Hillert[7], the critical grain radius R_c that separates growing and shrinking grains in a 3D system is related to the observed mean radius by:

$$R_c = \frac{8}{9}\bar{R} \tag{15}$$

Hillert also shows that the growth rate of the critical radius(and by Eq(15), of the average grain radius) is given by:

$$\frac{dR_c^2}{dt} = \frac{1}{4}M \tag{16}$$

which leads to the parabolic law:

$$R_c^2 - R_{c0}^2 = \frac{1}{4}Mt \tag{16a}$$

Combining Eqs((15) and (16) with Eq(3) permits the growth parameter M to be related to the measured grain growth constant:

$$k = \left(\frac{8}{9}\right)^2\left(\frac{1}{4}\right)M = 0.198M \tag{17}$$

The grain size distribution and the individual grain velocities are related by a continuity equation. The product $F\dot{R}$ is a flux of grains in grain-size space. The continuity equation is:

$$\frac{\partial F}{\partial t} = -\frac{\partial}{\partial R}(F\dot{R}) \tag{18}$$

Using this equation, Hunderi and Ryun[8] show how prescription of the individual grain-growth law(such as Eq(14)) determines F(R), or vice versa.

A major feature of the grain size distribution is that it is time-invariant if expressed in terms of

the size variable

$$u = \frac{R}{R_c} \tag{19}$$

The distribution function in terms of u is related to that in terms of R by:

$$f(u)du = F(R)dR$$

or

$$F(R) = f(u)\frac{du}{dR} = \frac{f(u)}{R_c} \tag{20}$$

The Hillert distribution function for 3-D grains is:

$$f(u) = 24e^3 \frac{u}{(2-u)^5} \exp\left(-\frac{6}{2-u}\right) \tag{21}$$

This distribution function is properly normalized to unity:

$$\int_0^2 f(u)du = 1 \tag{22}$$

Note that in normal grain growth, no grains larger than twice the critical size R_c exist.

Figure 4 shows the Hillert distribution(dotted curve) compared with the lognormal distribution proposed by Feltham[6](solid line) and a computer simulation(histogram). The dashed line is another theoretical model. Although available experimental data favor the computer simulations or the lognormal distribution, Hillert's theory, which is too sharply peaked, will be used in the following analysis because it contains only one parameter(M), which is directly obtainable from the experimental grain-growth constant by Eq(17).

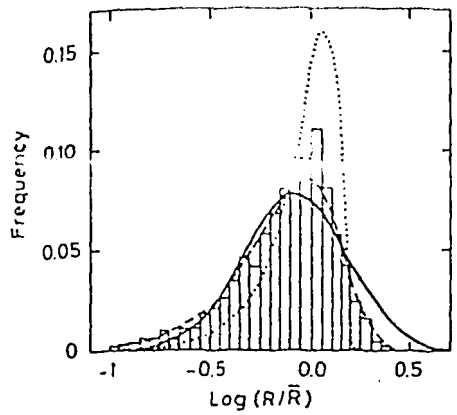

Fig. 4 Grain-size distribution functions. Hillert's is the dotted line. After Ref. 5.

The total number of grains per unit volume(N) is obtained by requiring that the grain system be space-filling:

$$1 = N\int_0^{2R_c}\left(\frac{4}{3}\pi R^3\right)F(R)dR = \frac{4}{3}\pi R_c^3 N\int_0^2 u^3 f(u)du$$

or

$$N = \frac{1}{\frac{4}{3}\pi R_c^3 E} \tag{23}$$

where E is the integral in the last term of the previous equation. It can be obtained numerically.

Growth Trajectories

The growth equation, Eq(14), is rewritten in terms of the dimensionless variables:

$$\mathcal{R} = \frac{R}{R_{c0}} \tag{24}$$

$$\tau = \frac{Mt}{R_{c0}^2} \tag{25}$$

Using Eq(16a) for R_c, Eq(14) becomes:

$$2\mathcal{R}\frac{d\mathcal{R}}{d\tau} = \left(\frac{\mathcal{R}}{\sqrt{1+\frac{\tau}{4}}} - 1\right) \tag{26}$$

where the initial condition is:

$$\mathcal{R} = u_0 \quad \text{at} \quad \tau = 0 \tag{27}$$

and $u_0 = R(\tau=0)/R_{c0}$ is the initial radius of the grain in question relative to the critical radius at $\tau=0$. Note that $0 \le u_0 \le 2$.

Following Hillert[7], new variables are defined by:

$$\mathcal{R} = e^{\tau'/2}u \tag{28}$$

where

$$\tau' = \ln(1+\tau/4) \tag{29}$$

This transformation converts Eq(26) to:

$$2u\frac{du}{d\tau'} = -(2-u)^2 \tag{30}$$

Equation(30) can be integrated directly to yield:

$$2\left[\frac{1}{2-u_0} - \frac{1}{2-u}\right] - \ln\left(\frac{2-u}{2-u_0}\right) = \frac{\tau'}{2} \tag{31}$$

The grain growth trajectory for a specified value of u_0 is calculated as follows: For each value of τ, τ' is determined from Eq(29); u is determined by solving Eq(31); $\mathcal{R}$ is determined from eq(28).

The growth trajectory plot according to the Hillert model is presented graphically in Fig. 5. All grains eventually disappear. However, those which initially are larger than R_{c0} first increase in size. No grain size ever exceeds twice the critical value.

The time for the grain to disappear, τ_f, is obtained by setting u = 0 in Eq(31):

$$\frac{2}{2-u_0} - \ln\left(\frac{2}{2-u_0}\right) = \frac{1}{2}\ln\left(1+\frac{\tau_f}{4}\right) \tag{32}$$

III GAS RELEASE TO GRAIN BOUNDARIES

Multigroup Formulation

This section outlines a method for calculating the fractional release of fission gas to the grain boundaries of the fuel at a specified time t. The initial grain population is characterized by the critical grain radius R_{c0} (or equivalently, the initial mean grain radius $\overline{R}_0$) and the grain growth constant M, which is related to the measured parabolic grain growth constant k by Eq(17). The distribution of grain sizes is given by Eq(21).

The initial distribution is divided into i_{tot} groups, each characterized by a minimum and a maximum radius, R_{imin0} and R_{imax0}, respectively. The average initial radius of the grains in group i is:

$$\overline{R}_{i0} = \int_{R_{imin0}}^{R_{imax0}} RF(R)dR \tag{33}$$

The i_{tot} groups can be divided into two classes. Grains in the first class, designated as class I, disappear from the microstructure at the specified final time. Class I contains the groups with $1 \le i \le j$. The maximum initial radius of group j is chosen such that the final radius of a grain of this size just vanishes at $\tau = Mt/R^2_{c0}$. It is given by:

Fig. 5 Grain growth trajectories

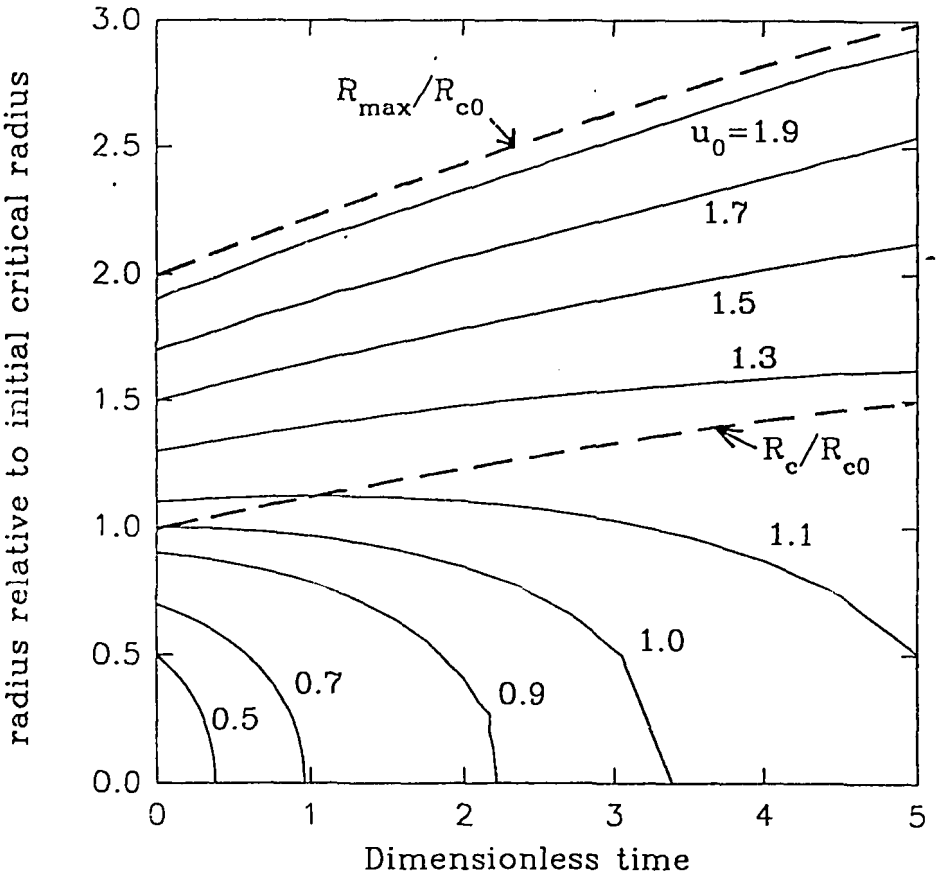

$$\frac{2}{2-\frac{R_{jmax0}}{R_{c0}}} - \ln\left(\frac{2}{\frac{R_{jmax0}}{R_{c0}}}\right) = \frac{1}{2}\ln\left(1+\frac{\tau}{4}\right) \tag{34}$$

The remaining group boundaries are chosen arbitrarily to cover the entire range of initial grain sizes.

Starting from this initial grouping of grain sizes, the mean radii of the i_{tot} groups evolve with time in the manner sketched in Fig. 6, which assumes j=3 and $i_{tot} = 8$. The mean radii characterizing the grains in each group $\overline{R}_i$ change with time according to Eq(31), with the intermediate variables τ' and u related to $\overline{R}_i$ and τ by Eqs(24), (28) and (29).

Gas Release from the Class I grains

The fission gas that was originally contained in the grains that disappear in time τ_f(Class I groups) is delivered to the grain boundaries of the solid. The fractional release from the Class I groups is equal to the volume fraction of these grains in the solid:

$$f^{I}_{r,gb} \doteq \frac{\int_0^{u_j} u^3 f(u)du}{\int_0^{2} u^3 f(u)du} = \frac{1}{E}\int_0^{u_j} u^3 f(u)du \tag{35}$$

where

$$u_j = \frac{R_{jmax0}}{R_{c0}} \tag{36}$$

In Fig. 2, for example, the small grain designated with the minus sign in stage (a) vanishes at stage (f). All of the fission gas originally in this grain is collected in the nearby grain boundaries.

Diffusion analysis of Class II Grains

The remaining grain groups $j+1 \le i \le i_{tot}$ that survive to time τ_f are designated as class II groups. Some of these groups grow and some shrink during this period. All remain distinct entities. Their characteristic sizes $\overline{R}_i$ change with time as indicated above.

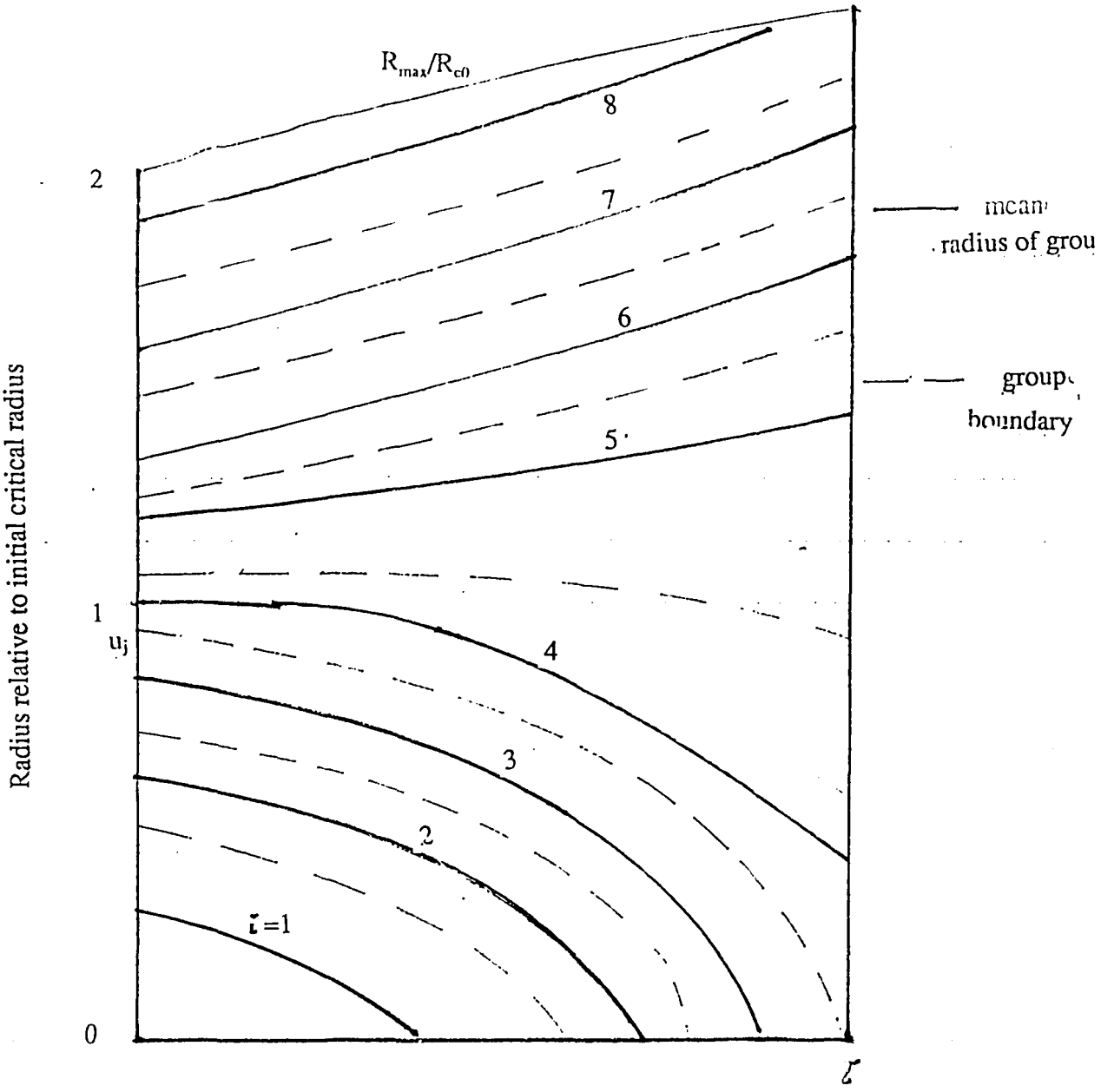

Fig. 6 Group Trajectories

Fission gas behavior in class II grains is one of diffusion in a sphere with a moving boundary. The governing equations are:

$$\frac{\partial C}{\partial t} = D\frac{1}{r^2}\frac{\partial}{\partial r}\left(r^2\frac{\partial C}{\partial r}\right) \tag{37}$$

for $0 \le r \le R(t)$. The initial condition for postirradiation annealing is:

$$C(r,0) = 1 \tag{38}$$

and the boundary conditions are:

$$C(R(t),t)) = 0 \tag{39}$$

$$\left(\frac{\partial C}{\partial r}\right)_{r=0} = 0 \tag{40}$$

Where C is the concentration of fission gas in the sphere and R(t) is the time-dependent boundary radius. It represents the mean radius of the grains in a particular group, $\overline{R}_i(t)$, but the bar and the subscript i are omitted for simplicity.

Let:

$$X = \frac{r}{R(t)} \tag{41}$$

$$\theta = D\int_0^t \frac{dt'}{R^2(t')} \tag{42}$$

and

$$C(r,t) = W(X,\theta) \tag{43}$$

Using the chain rule of differentiation:

$$\frac{\partial C}{\partial t} = \frac{\partial W}{\partial X}\frac{\partial X}{\partial t} + \frac{\partial W}{\partial \theta}\frac{\partial \theta}{\partial t} = -\frac{r}{R^2(t)}\frac{\partial R}{\partial t}\frac{\partial W}{\partial X} + \frac{D}{R^2(t)}\frac{\partial W}{\partial \theta}$$

$$\frac{\partial C}{\partial r} = \frac{\partial W}{\partial X}\frac{\partial X}{\partial r} + \frac{\partial W}{\partial \theta}\frac{\partial \theta}{\partial r} = \frac{1}{R(t)}\frac{\partial W}{\partial X}$$

Substitution into Eq(37) yields:

$$\frac{\partial W}{\partial \theta} = \frac{1}{X^2}\frac{\partial}{\partial X}\left(X^2\frac{\partial W}{\partial X}\right) + \frac{1}{2}g(\theta)X\frac{\partial W}{\partial X}, \qquad 0 = X = 1 \tag{44}$$

where:

$$g(\theta) = \frac{1}{D}\frac{d}{dt}[R^2(t)] \tag{45}$$

The initial condition is:

$$W(X,0) = 1 \tag{46}$$

and the boundary conditions are:

$$W(1,\theta) = 0 \tag{47}$$

$$\left(\frac{\partial W}{\partial X}\right)_{X=0} = 0 \tag{48}$$

The moving boundary condition problem has been converted to a fixed boundary problem with a convective term(the last term in Eq(44)) in the diffusion equation. This problem has been solved analytically by Chambre[9] for the case $R(t) = R_o + k't$, where k' is a specified constant.

$$g(\theta) = \gamma[(u(\theta) - 1] \tag{49}$$

where

$$\gamma = \frac{M}{D} \tag{50}$$

is a dimensionless parameter reflecting the relative importance of grain growth and fission gas diffusion.

The variation of u with θ is derived in the Appendix. The result is:

$$\gamma\theta = 4\left(\frac{1}{2-u_0} - \frac{1}{2-u}\right) - 2\left[\ln\left(\frac{2-u_0}{u_0}\right) - \ln\left(\frac{2-u}{u}\right)\right] \tag{51}$$

With Eq(44) solved(numerically), the average concentration in the sphere is given by Eq(11) in dimensionless form:

$$\overline{C} = 3\int_0^1 X^2 W(X,\theta)dX \tag{52}$$

The dimensionless time τ of Eq(25) is related to θ of Eq(42) by:

$$\theta = \frac{1}{\gamma}\int_0^\tau \frac{d\tau'}{\mathcal{R}^2(\tau')} \tag{53}$$

The dimensionless sphere radius $\mathcal{R}(\tau)$ is obtained from Fig. 5 and the integration is performed numerically.

The fractional release from all of the grain groups in class II is given by:

$$f^{II}_{r,gb} = 1 - \sum_{i=j+1}^{i_{tot}} V_i \overline{C}_i \tag{54}$$

where V_i is the volume fraction of grains in group i:

$$V_i = N\int_{R_{imin}}^{R_{imax}} \frac{4}{3}\pi R^3 F(R)dR = \frac{1}{E}\int_{u_{imin}}^{u_{imax}} u^3 f(u)du \qquad (55)$$

where Eqs(19) and (23) have been employed. The integration limits in Eq(55) are obtained from the solutions of Eqs(29) and (31) with u_0 given by R_{imax0}/R_{c0} and R_{imin0}/R_{c0} for the upper and lower limits, respectively.

APPENDIX

Substituting Eq(29) into Eq(31) yields:

$$g(u) = \ln\left(1+\frac{1}{4}\tau\right) \qquad (A-1)$$

where

$$g(u) = 4\left(\frac{1}{2-u_0} - \frac{1}{2-u}\right) - 2\ln\left(\frac{2-u}{2-u_0}\right) \qquad (A-2)$$

Using Eqs(28) and (29), Eq(53) becomes:

$$\theta = \frac{1}{\gamma}\int_0^{\tau}\frac{d\tau'}{[u(\tau')]^2\left(1+\frac{1}{4}\tau'\right)} \qquad (A-3)$$

where Eqs(28) and (29) have been used. Changing the variable of integration from τ to u using Eq(A-1) yields:

$$\theta = \frac{4}{\gamma}\int_{u_0}^{u}\left(\frac{dg}{du'}\right)\frac{du'}{(u')^2} \qquad (A-4)$$

With the derivative of g obtained from Eq(A-2), Eq(51) of the text results.

REFERENCES

1. A. H. Booth, Atomic Energy of Canada, Ltd., Report No. AECL-496 (1957)

2. R. Hargreaves and D. A. Collins, J. Brit. Nucl. Energy Soc., 15, 311 (1976)

3. E. E. Underwood, "Quantative Stereology", Addison Wesley, Mass. (1970)

4. J. Rest and A. W. Cronenberg, J. Nucl. Mater., **150**, 203 (1987)

5. H. V. Atkinson, Acta Metall. **36**, 469 (1988)

6. P. Feltham, Acta Metall., **5**, 97 (1957)

7. M. Hillert, Acta Metall., **13**, 227 (1965)

8. O. Hunderi and N. Ryum, J. Mater. Sci. **15**, 1104 (1980)

9. P. L. Chambre, J. Nucl. Mater. **18**, 167 (1966)